AC RESEARCH

Near-Infrared Spectrophotometric Monitoring of Stroke-Related Changes in the Protein and Lipid Composition of Whole Gerbil Brains

John M. Carney,† Warren Landrum,† Lisa Mayes, Yi Zou,‡ and Robert A. Lodder*

College of Pharmacy, Division of Medicinal Chemistry and Pharmaceutics, University of Kentucky Medical Center, Lexington, Kentucky 40536-0082

Strokes are a critical problem in the U.S. that affect more than 500 000 people annually. Research into the causes of stroke and testing of drug therapies to reduce ischemic and postischemic damage to the brain is frustrated by an inability to continuously follow the physical and chemical events that occur during ischemia and reperfusion in vivo. Near-IR spectrometry is used in this paper to observe stroke-induced changes in the lipids and proteins of whole brain samples and in intact subjects. The examination of whole brains is made possible by a combination of hardware and software techniques designed to make the sample presentation to the spectrometer more reproducible. Near-IR spectrophotometry of brain tissue discriminates between adult (3–4 months of age) and aged (18–20 months of age) brains as well as between brains exposed to 5- and 10-min ischemia. The near-IR analytical method has many applications in aging and stroke research, including the noninvasive determination of age from brain spectra obtained transcranially, simultaneous multicomponent analysis of lipids and proteins, and quantification of edema.

INTRODUCTION

Strokes are a serious problem in the U.S. that affect over 500 000 people annually.[1] Approximately 30% of the affected individuals succumb to the disease each year, while another 20–30% suffer permanent disability because of the disease. Research into the causes of stroke and the development and testing of drug therapies to reduce ischemic and postischemic damage to the brain is hampered by an inability to identify and follow the physical and chemical events that occur during ischemia and reperfusion in vivo. While methods such as magnetic resonance imaging (MRI) penetrate tissue to provide some chemical and spatial information on living systems, extraction of molecular information is difficult, expensive, and time-consuming. In addition, repetitive monitoring of critical patients is not possible except at the bedside, far from the MRI. Separation methods such as HPLC and capillary electrophoresis can provide more accurate information about the molecules present in tissue samples at a greatly reduced cost. However, separation techniques cannot be applied noninvasively and repeatedly to the same animal research subjects and are not applicable to patients. (Invasive procedures, including surgical procedures to enable the controlled initiation of an ischemic event, often generate strokes themselves, complicating interpretation of the results of controlled studies of stroke. Strokes that occur unexpectedly in test animals before the planned ischemic event require the use of a larger sample population than might otherwise be required.) Computerized axial tomography (CAT) scanners using X-rays and MRI instruments are not particularly portable or rugged, making them somewhat inaccessible to researchers and clinicians.

Near-infrared spectrometry has historically been used to monitor fat and protein in agricultural products.[2] Similar near-infrared techniques have been employed more recently in the study of animal systems.[3] In this paper, near-IR spectrometry is used to examine stroke-induced changes in the lipids and proteins of whole gerbil brains. Near-IR spectrometry is well-suited for this work because tissue penetration by near-IR light is good, excellent S/N ratios can be obtained in near-IR measurements, and discrimination between various types of brain constituents is possible because the near-IR signals arise from combinations and overtones of the fundamental IR bands of these constituents. The gerbil brain is an established animal model of stroke. In addition, the gerbil brain is enriched in polyunsaturated fatty acids. There are dramatic changes in fatty acid metabolism during the ischemia and reperfusion stages. The changes parallel

* Author to whom correspondence should be addressed. Telephone: (606)257-9232.
† Present address: Department of Pharmacology, College of Medicine, University of Kentucky Medical Center, Lexington, KY 40536.
‡ Present address: Department of Chemistry, University of Kentucky, Lexington, KY 40506.

(1) Zivin, J. A.; Choi, D. W. Stroke therapy. *Sci. Am.* **1991**, *265* (1), 56–63.

(2) Wetzel, D. L. Near-infrared reflectance analysis. *Anal. Chem.* **1983**, *55*, 1165A–1176A.

(3) Cassis, L. A.; Lodder, R. A.; Ciurczak, E. W. Arterial analysis with a novel near-IR fiber optic probe. *Spectroscopy* **1990**, *5* (7), 18–16.

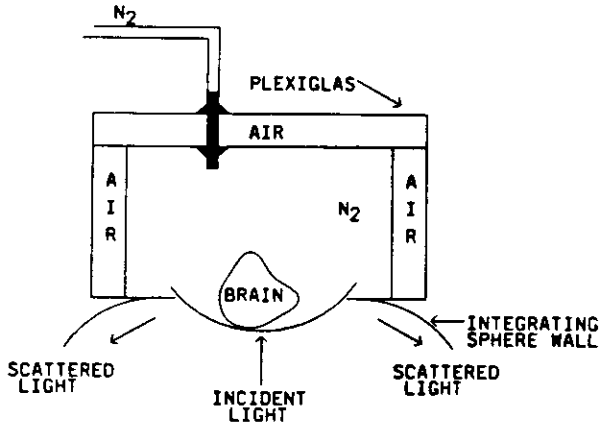

Figure 1. Sample compartment constructed from clear Plexiglas to hold excised frozen brains.

the hypothesized series of free radical and altered enzymatic events that occur during transient ischemia and reperfusion in the brain of man. Finally, the skull of the gerbil is relatively thin, making near-IR spectrometry of the brain readily achievable in vivo with common spectrometers of moderate light intensity.

In order to understand the early changes in lipid and protein metabolism following stroke and trauma, we have developed animal models to recreate these changes. The examination of whole brains was made possible by a combination of hardware modifications and mathematical techniques designed to make the sample presentation to the spectrometer quite reproducible. A refrigerated sample compartment with dry nitrogen purge was constructed for analysis of whole frozen brains (see Figure 1). The cooled compartment enabled repeated scans of frozen brains to be collected over time without thawing. The spectrophotometer itself was also purged with dry nitrogen gas, eliminating spectral artifacts associated with lipid/protein oxidation and atmospheric water vapor or other gases. A geometric noise filter removed spectral variations arising from position variation of the brain. The BEST and extended BEST algorithms, based on the BEAST,[4] which scales spectral vectors in multidimensional hyperspace with a directional probability, were used with a supercomputer to analyze the spectra collected.

In addition to changes observed in a stroke, previous literature suggests that there are age-related changes in the polyunsaturated fatty acid pool and in the state of protein oxidation within the central nervous system. The near-IR analytical method has many applications to this aging and stroke research, including (1) determination of age from brain spectra, (2) prediction of short-term memory deficit from the spectra of injured brains, (3) simultaneous multicomponent analysis of lipids and proteins, (4) quantification of edema, and, (5) transcranial scanning of the brain in vivo. Near-IR scanning of brains in vivo simplifies the testing of drug candidates by reducing the number of number of subjects required, by allowing each subject to be used as its own control, and by eliminating variance due to outlier subjects (such as those that have had a stroke before the experiment).

THEORY

A population **P** in a hyperspace **R** represents the universe of possible spectrometric samples (the rows of **P** are the individual samples, while the columns are the independent information vectors, such as wavelengths or energies). **P*** is a discrete realization of P based on a calibration set T, which has the same number of columns as **P*** and is chosen only once from **P** to represent as nearly as possible all the variations present in **P**.

P* is calculated using a bootstrap process by an operation $\kappa(\mathbf{T})$, and **P*** has parameters **B** and **C**, where **C** equals $E(\mathbf{P})$ and **B** is the Monte Carlo approximation to the bootstrap distribution. The expectation value, $E(\ )$, of **P** is the center of **P**, and **C** is a row vector with as many elements as there are columns of **P**.

Each new sample spectrum **X** is analyzed by an operation $\psi(\mathbf{T},\mathbf{B},\mathbf{X},\mathbf{C})$, which projects a discrete representation of the probability density of **P** in hyperspace by many-one mapping onto the vector connecting **C** and **X**. **X** and **C** have identical dimensions. The directional standard deviation (SD) σ is found from the projected probability density:

$$\sigma\left|\frac{\int_0^{\sigma}\left(\int_R \mathbf{P}^* \rightarrow \vec{CX}\right)}{\int_R \mathbf{P}^* \rightarrow \vec{CX}}\right| = 0.68 \qquad (1)$$

The integral over the hyperspace **R** is calculated from the center of **P** outward. The calculation of a skew-adjusted σ is based on a comparison of the expectation value $\mathbf{C} = E(\mathbf{P})$ and $\mathbf{C_T} = \mathrm{med}(\mathbf{T})$, the median of **T** in hyperspace (with the same dimensions as **C**) projected on the hyperline connecting **C** and **X**:

$$(\mathbf{C} - \mathbf{C_T}) \rightarrow \vec{CX} \qquad (2)$$

The result of the corrected projection is an asymmetric σ that provides two measures of the standard deviation along the hyperline connecting **C** and **X**:

$$\overset{+}{-}\sigma\left|\frac{\int_0^{+\sigma}\left(\int_R \mathbf{P}^* \rightarrow \vec{CX}\right)}{\int_R \mathbf{P}^* \rightarrow \vec{CX}}\right| = 0.34 \qquad (3)$$

in the direction of X in hyperspace, and

$$\overset{-}{-}\sigma\left|\frac{\int_0^{-\sigma}\left(\int_R \mathbf{P}^* \rightarrow \vec{CX}\right)}{\int_R \mathbf{P}^* \rightarrow \vec{CX}}\right| = 0.34 \qquad (4)$$

in the opposite direction along the hyperline connecting **C** and **X**. Skew-adjusted SDs can be used to calculate mean distances between spectra of different samples like those in Table I. When the different samples are each represented by a number of spectra and the two mean skew-adjusted SDs are less than 3, an alternative definition of σ can be profitably employed.

Given two calibration sets $\mathbf{P_1}^*$ and $\mathbf{P_2}^*$ with an equal number of elements n, it is possible to determine whether

Table I. Frozen Excised Gerbil Brains: Distance Between Sets of 10 Brains (in SDs)

	training set				
test set	YControl	Yi5r60	Yi10r60	OControl	Oi5r60
YControl[a]	−0.57	12.58	34.38	14.10	41.26
Yi5r60[b]	27.96	−0.42	8.18	18.92	11.47
Yi10r60[c]	44.42	7.78	−0.99	6.01	1.43[f]
OControl[d]	23.69	15.44	5.35	−0.66	11.02
Oi5r60[e]	19.43	1.29	−0.33[f]	0.66	−0.67

[a] YControl = adult control brains. [b] Yi5r60 = adult brains after 5-min ischemia and 60-min reperfusion. [c] Yi10r60 = adult brains after 10-min ischemia and 60-min reperfusion. [d] OControl = aged control brains. [e] Oi5r60 = aged brains after 5-min ischemia and 60-min reperfusion. [f] Only group indistinguishable from another.

(4) Lodder, R. A.; Hieftje, G. M. Quantile BEAST attacks the false-sample problem in near-infrared reflectance analysis. *Appl. Spectrosc.* 1988, *42*, 1351–1365.

P_1^* and P_2^* are drawn from the same population even if σ_1 and σ_2 are less than 3 using quantile–quantile (QQ) plots and a simple correlation test statistic:[5]

$$\rho(\{\int_R \mathbf{P}_1^*\}\{\int_R \mathbf{P}_1^*\} \bigcup \{\int_R \mathbf{P}_2^*\}) \quad (5)$$

A bootstrap method is employed to set confidence limits on ρ. The central 68% confidence interval on ρ is also used to calculate σ_ρ by calculating the difference between ρ from sets 1 and 2 and ρ from set 1 and the mean of a set of replications of itself. This difference is then divided by the standard deviation of the set of replications of set 1 to give σ_ρ. σ_ρ is a distance in SDs that is different from σ and is more sensitive to small differences in location and scale between P_1^* and P_2^*.

To reduce the effects of nonrandom noise on measurements in hyperspace, each row of P^* is calculated from three spectra of an individual brain sample by a filtering algorithm based on the Euclidean distances between the three spectral points in hyperspace. The Euclidean filtering algorithm performs multiplicative scatter correction on the three spectra from each sample, measures the distance between each pair of points, and averages the coordinates of the two closest points to form a row of P^*. In most cases, the Euclidean filter changes the spectral data only slightly and functions only to catch the occasional gross outlier that might be generated by sample motion or specular reflectance from a large ice crystal.

EXPERIMENTAL SECTION

The nonparametric BEST algorithm summarized in eqs 1–5 has been tested extensively with normally distributed spherical ($N(0,1)$) synthetic spectral data in hyperspace and has been shown to produce excellent results.[4,6] Representative quantile–quantile plots for the simulations have been published.[6] Because spectral data obtained from biological systems are seldom normally distributed in hyperspace, however, the BEST equations were tested with synthetic spectral data from elliptical (n-variate normal) and skewed distributions before the equations were applied to the analysis of spectral data from the animal model. The elliptical distributions in hyperspace had a major axis 2 SDs long, while the minor axes were all 1 SD long. The skewed distributions in hyperspace had a major axis with a skewness (B_1) of 1 (±0.05) and minor axes that were all 1 SD long. Differences between training sets and test sets were reflected in differences in location, scale (size), and skew (shape) of the synthetic spectral distributions. The ability of the equations to detect changes in spectra without making parametric assumptions was verified, and bias and RSD of the BEST metric in eq 5 for typical data sets were calculated.

Spectra of both frozen and living gerbil brains were obtained to test the following hypotheses:

(1) There are inherent chemical differences in the brain tissue of adult (3–4 months) and aged (18–20 months) gerbils, and these differences are detectable in the near-IR spectral region.

(2) Aged gerbils show an increase in the level of oxidatively modified protein and lipid in their brain tissue that appears as protein carbonyl in the near-IR.[7]

(3) Near-IR spectrometry can characterize nondestructively changes in saturated, monounsaturated, and polyunsaturated fatty acids.

(4) Peroxidation of fatty acids occurs during reperfusion of the brain following ischemia, which leads to a saturation and/or cis–trans isomerization of fatty acids that is detectable in the near-IR.

(5) Ischemia/reperfusion injuries lead to edema (an increase in intracellular water) detectable in the near-IR.

Materials. A commercial near-IR spectrophotometer (Bran+ Luebbe, New York) similar to that used in our previous studies[8] was modified to include a subfreezing insulated sample compartment (see Figure 1) that was purged (along with the spectrometer itself) with dry nitrogen gas boil-off from a 100-L dewar. The sample compartment was constructed from a double layer of Plexiglas to permit the sample position, optics, and temperature to be easily observed. The sample compartment had a hinged lid to allow sample insertion. The room in which the spectrophotometer was located was completely darkened during scans. The rate of nitrogen flow to the spectrometer and sample compartment was increased by placing a coil of copper tubing in the liquid nitrogen dewar through which dry compressed air flowed. A drop of water placed on the sample holder over the beam port froze in less than 5 s when the nitrogen flow was properly adjusted. Each frozen brain was repositioned in the compartment and scanned three times. The Plexiglas compartment was removed for in vivo brain scans, which were obtained at a tissue temperature near 37 °C. No sample preparation was required to scan excised frozen brains. In vivo brain scanning was preceded only by shaving the hair on the gerbil head.

Spectrophotometric reference standards of nine fatty acids relevant to brain chemistry were obtained from Matreya (Pleasant Gap, PA) (see Figure 2a–i). The nine acids were scanned neat to provide spectral references using a monochromator system with a concave holographic grating (LT Industries, Rockville, MD). The acids were n-hexadecanoic acid (16:0) (no. of carbon atoms: no. of carbon–carbon double bonds), n-octadecanoic acid (18:0), oleic acid (18:1), elaidic acid (18:1), linoleic acid (18:2), linoelaidic acid (18:2), arachidonic acid (20:4), docosahexaenoic acid (22:6), and nervonic acid (24:1). The naturally occurring acids are all cis in the absence of a pathological condition. Elaidic acid is trans at C-9, and linoelaidic acid is trans at C-9 and C-12.

Synthetic mixing of the fatty acid reference spectra by vector addition was performed to estimate the appearance of the total fatty acid spectrum of the gerbil brain. The nine fatty acid spectra were expressed in vector form, with the length of each vector proportional to the estimated amount[9] of that fatty acid present in gerbil brain tissue. The resulting vector sum appears in Figure 3 and was used to find the spectral regions of interest for scanning.

The software used to collect and analyze spectral data was written in Speakeasy IV Epsilon+ and Zeta, respectively. Data were collected on a MicroVAX II computer using the Speakeasy programs and analyzed on an IBM 3090-600J parallel vector supercomputer using the same set of Speakeasy programs.

Subjects. Adult and aged Mongolian gerbils were obtained from Tumblebrook Farms (West Brookfield, MA).

Methods. The gerbils were sacrificed by decapitation, and their brains were quickly removed on a cold stage. The brains were frozen rapidly by immersion in liquid nitrogen following dissection from the gerbils. The brains were stored at −70 °C until scanning. The brains were kept frozen throughout the scanning process to minimize spectral effects resulting from temperature changes. Each brain was repositioned and scanned three times in the holder to reduce positioning artifacts in the spectra. The final spectrum retained of each brain was the Euclidean-filtered average of the three scans.

Surgical Procedures. The two procedures conducted on each gerbil have been described in detail previously.[10] The animals are anesthetized with pentobarbital (40 mg/kg) for the evaluation of stroke-induced changes in brain tissue. The first procedure is conducted 48 h before ischemia is induced. This initial procedure loops a suture around each common carotid artery of the gerbil and exteriorizes the free ends through a double-

(5) Galante, L. G.; Brinkley, M. A.; Lodder, R. A. Near-IR spectrometry of microorganisms in liquid pharmaceuticals. *Anal. Chem.* **1990**, *62*, 2514–2521.

(6) Lodder, R. A.; Hieftje, G. M. Detection of subpopulations in near-infrared reflectance analysis. *Appl. Spectrosc.* **1988**, *42*, 1500–1512.

(7) Oliver, C. N.; Starke-Reed, P. E.; Stadtman, E. R.; Liu, G. J.; Carney, J. M.; Floyd, R. A. Oxidative damage to brain proteins, loss of glutamine synthetase activity, and production of free radicals during ischemia/reperfusion-induced injury to gerbil brain. *Proc. Natl. Acad. Sci. U.S.A.* **1990**, *87*, 5144–5147.

(8) Lodder, R. A.; Selby, M.; Hieftje, G. M. Detection of capsule tampering by near-infrared reflectance analysis. *Anal. Chem.* **1987**, *59*, 1921–1930.

(9) Hamayoun, P.; Benttejac, M.; Lecerf, J.; Bourre, J. M. Uptake and utilization of double-labeled high-density lipoprotein sphingomyelin in isolated brain capillaries of adult rats. *J. Neurochem.* **1989**, *53*, 1031–1035.

(10) Cao, W.; Carney, J. M.; Duchon, A.; Floyd, R. A.; Chevion, M. Oxygen free radical involvement in ischemia and reperfusion injury to brain. *Neurosci. Lett.* **1988**, *88*, 233–238.

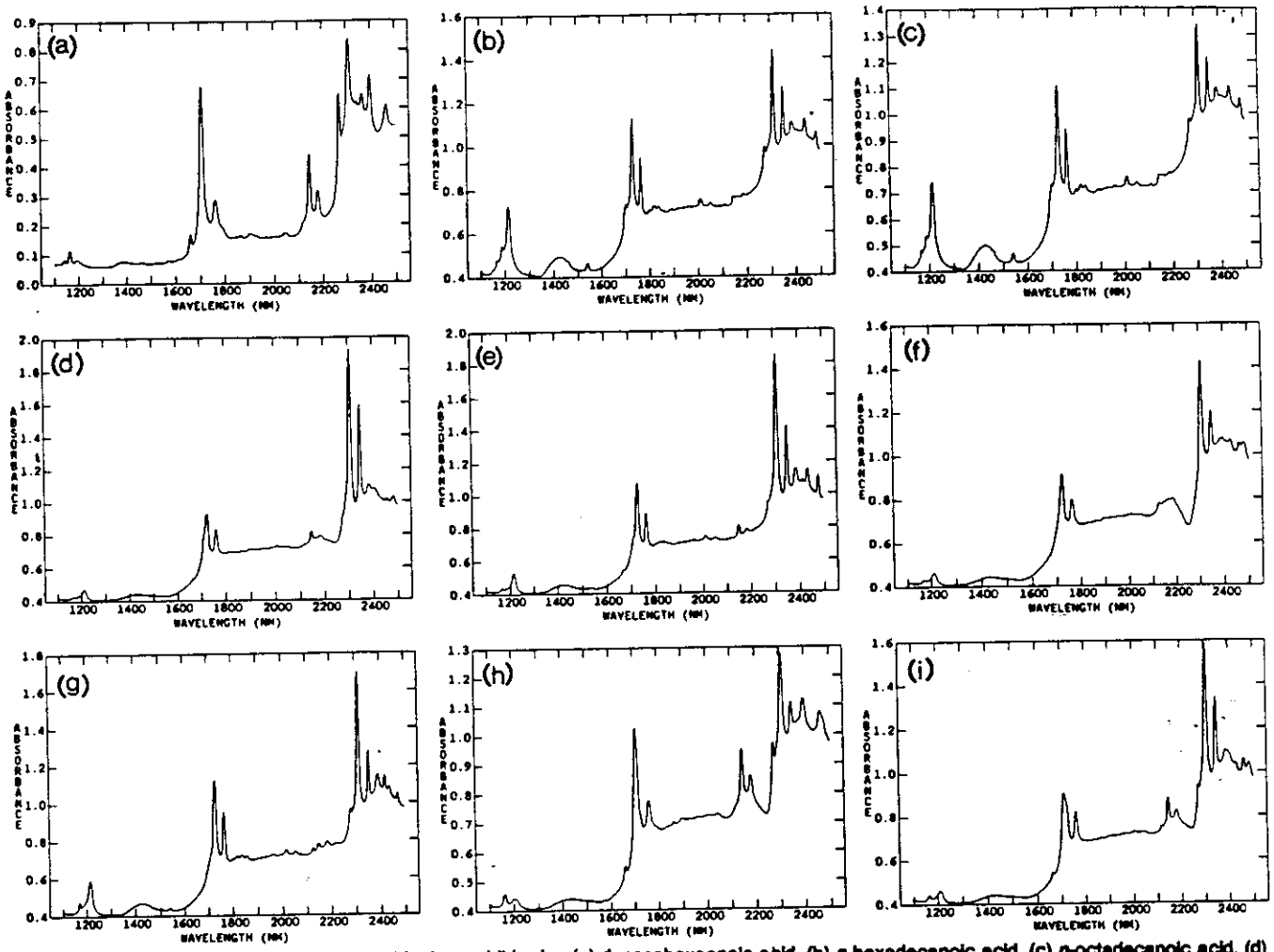

Figure 2. Spectra of nine fatty acids found in the gerbil brain: (a) docosahexaenoic acid, (b) *n*-hexadecanoic acid, (c) *n*-octadecanoic acid, (d) oleic acid, (e) nervonic acid, (f) linoelaidic acid, (g) elaidic acid, (h) arachidonic acid, and (i) linoleic acid.

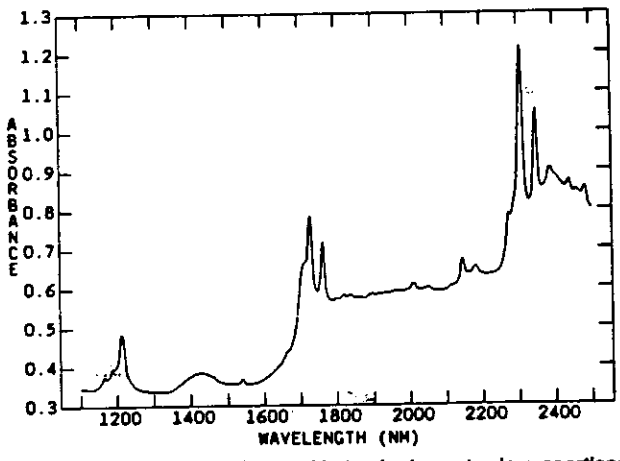

Figure 3. Vector sum of fatty acid standard spectra in proportions found in the living brain.

lumen catheter to permit the controlled induction of ischemia. The catheter is fixed in the dorsum of the neck with cyanoacrylate adhesive. Ischemia (stroke) is produced 48 h later in the second procedure by tightening the sutures and closing the carotid arteries against the septa of the double-lumen catheters for a predetermined time period (the duration of ischemia). When the suture is loosened and removed, the reperfusion period begins. The duration of reperfusion is also predetermined and controlled. The final procedure is decapitation and the removal of the entire brain, which is rapidly frozen in liquid nitrogen. The excised brain is scanned after freezing.

Specific gravity of gerbil brains is determined by suspending a piece of the nonfrozen excised brain in a bromobenzene/kerosene density-gradient column.[11] Edema is inversely correlated to specific gravity.

In Vivo Brain Scanning. The only additional sample preparation step employed in in-vivo brain scanning was the shaving of the gerbil heads over the cerebral region of the brain. Edema was observable in near-IR spectra from a test subject without shaving (see Figure 4). Shaving tended to increase the recorded signals from water, lipid, and protein bands, probably through a reduction in light losses caused by scattering from the hair.

Five hypotheses were addressed experimentally in this study as follows:

(1) The hypothesis that near-IR spectrometry can characterize nondestructively changes in saturated, monounsaturated, and polyunsaturated fatty acids was tested with 50 frozen gerbil brains. The spectra obtained from these samples were compared to spectra of eight different fatty acid standards.

(2) The hypothesis that there are inherent chemical differences in the brain tissue of adult and aged gerbils that are detectable in the near-IR was tested first with six frozen brains from gerbils that did not experience deliberate ischemic events (three that were 3-months old when sacrificed and three that were approximately 18-months old when sacrificed). This preliminary experiment suggested differences that were confirmed in a second experiment using 20 frozen brains also from gerbils that did not experience any deliberate ischemic events (10 adult and 10 aged).

(11) Gonzalez-Darder, J.; Canadas-Rodriguez, D. Effects of cervical spinal cord stimulation in experimental ischaemic oedema. *Neurol. Res.* 1991, *13* (4), 229–232.

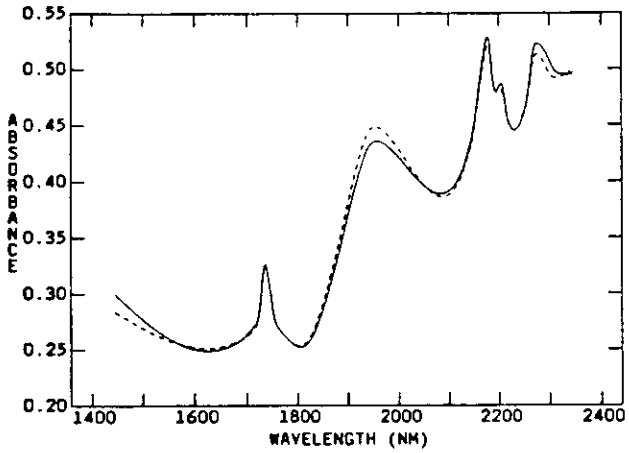

Figure 4. In vivo spectra of gerbil brain, obtained transcutaneously without shaving before ischemia (solid line) and after 1-h reperfusion (dashed line). The gerbil was from the aged group and underwent 10-min ischemia before reperfusion.

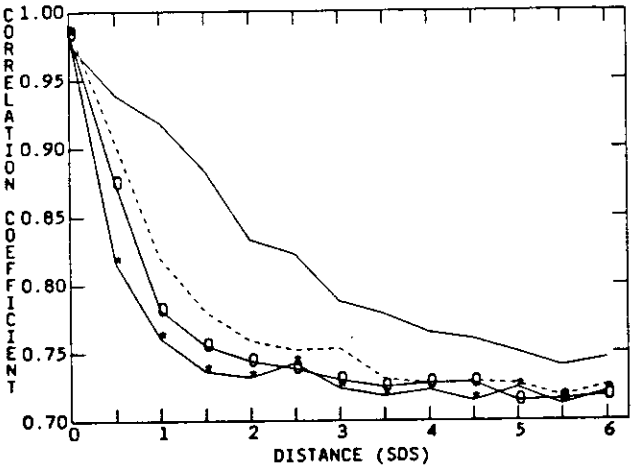

Figure 5. Correlation ρ as a function of the distance in SDs between a synthetic training set and a test set. Both the training set and the test set are elliptical and are represented by 1000 bootstrap replicates in a 20-D hyperspace. The training set and the test set each contained 10 samples (solid line), 50 samples (dashed line), 100 samples (dashed line with O), or 200 samples (dashed line with asterisks).

(3) The hypothesis that aged gerbils show an increase in the level of oxidatively modified protein and lipid in their brain tissue that appears in the near-IR was tested with 20 frozen brains from gerbils that did not experience any deliberate ischemic events.

(4) The hypothesis that peroxidation of fatty acids occurs during reperfusion of the brain following ischemia and that a free-radical mechanism leads to a saturation and/or cis–trans isomerization of fatty acids that is detectable in the near-IR was tested with 50 frozen brains.

(5) The hypothesis that ischemia/reperfusion injuries lead to edema detectable in the near-IR was tested with 50 frozen brains and four brains scanned noninvasively in vivo.

RESULTS AND DISCUSSION

The results of the theroretical studies performed on the supercomputer are summarized in Figures 5–8. Figure 5 depicts the behavior of the correlation ρ as a function of the distance in SDs between a synthetic training set and a test set. Both the training set and the test set are elliptical and are represented by 1000 bootstrap replicates in a 20-dimensional (20-D) hyperspace. The correlation between the training set and the test set drops as the two sets are gradually moved apart in hyperspace. A confidence limit calculated on ρ is used to decide when the training set and the test set

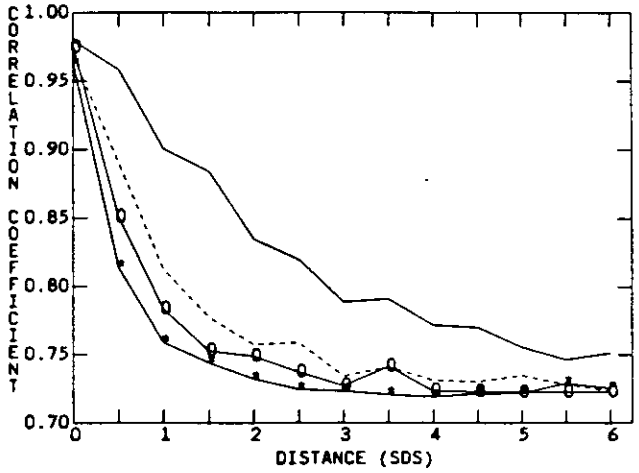

Figure 6. Correlation ρ as a function of the distance in SDs between a synthetic training set and a test set. Both the training set and the test set are skewed ($B_1 = 1$ on the major axis) and are represented by 1000 bootstrap replicates in a 20-D hyperspace. The training set and the test set each contained 10 samples (solid line), 50 samples (dashed line), 100 samples (dashed line with O), or 200 samples (dashed line with asterisks).

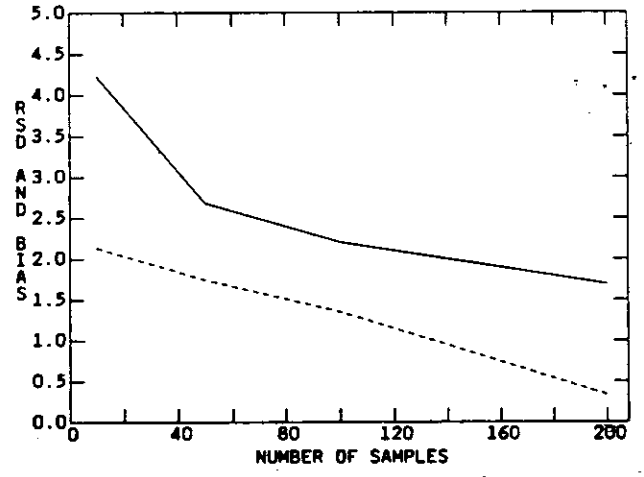

Figure 7. Bias (solid line) and RSD (dashed line) of ρ as a function of the number of training and test samples employed, calculated from six repeated trials with $B = 1000$ replicates of the training set and the test set. Each set was a random sample from an elliptical distribution in 20-D hyperspace.

occupy a different region in hyperspace with 98% confidence. Training set confidence limits on ρ are typically between 0.90 and 0.95. As the number of training samples increases, the sensitivity of eq 5 (reflected in the slope of the line) increases. Equation 5 is very sensitive to small changes in the location of spectral sets in hyperspace and usually treats larger displacements as identical in magnitude (particularly when a large number of training and test samples are available).

Figure 6 depicts behavior similar to Figure 5 and is also based on 1000 bootstrap replicates in a 20-D hyperspace. Figure 6 is calculated from skewed training and test sets, however, making the use of more conventional discriminant metrics like the Mahalanobis metric impossible. Equation 5 functions as admirably in Figure 6 as it did in Figure 5 in spite of the change in distributional assumptions.

The bias and relative standard deviation (RSD) of ρ for typical numbers of training and test samples are given by percentages in Figure 7. [Bias and RSD are used in the usual sense: bias is the expected value of $(T - \Theta)$ for T as a point estimator of Θ, and RSD is the positive square root of the variance divided by T.] The values graphed in Figure 7 are calculated from six repeated random samples from elliptical

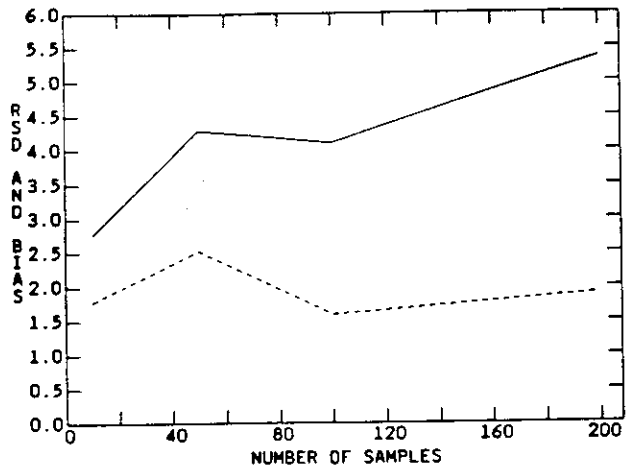

Figure 8. Bias (solid line) and RSD (dashed line) of ρ as a function of the number of training and test samples employed, calculated from six repeated trials with B = 1000 replicates of the training set and the test set in 20-D hyperspace. Each set was a random sample from a skewed distribution (B_1 = 1 on the major axis).

distributions with B = 1000 replications in a 20-D hyperspace. The smallest quantity of synthetic samples used in training and test sets (10) produced the largest bias and RSD of ρ, as expected. Nevertheless, the bias was only 4.2%, and the RSD was only 2.2%. The bias and RSD continue to drop steadily as more samples are used.

Figure 8 gives the bias and RSD for ρ calculated from skewed distributions. The bias and RSD for ρ are approximately equal to those calculated from unskewed training and test sets, in spite of the change in distributional assumptions. The RSD is relatively unaffected by the quantity of training and test samples, while the bias seems to increase very slowly. The values graphed in Figure 8 are calculated from six repeated random samples from skewed distributions with B = 1000 replications in a 20-D hyperspace.

Testing Fatty Acids Nondestructively To Determine Whether the Acids Are Saturated, Monounsaturated, or Polyunsaturated. Spectra of the fatty acids appear in Figure 2a–i. The cis fatty acids lack peak structure in the 1800–1875-nm region and have a pair of peaks near 2150 and 2190 nm. Elaidic acid (the trans isomer of oleic acid) has four peaks in the 1800–1875-nm region. The saturated fatty acids have three peaks in the 1800–1875-nm region, a third peak in the pair at 1710 and 1190 nm, and a distinctive peak structure at 2150 nm. Although some spectra appear superficially similar, the presence of slightly different peak structures as well as dramatically different ratios of peak areas makes simple the near-IR spectrophotometric identification of unique fatty acids in vitro. The trans fatty acid and the saturated fatty acids have more low energy peak structure than the cis fatty acids. An increase in low energy peaks is noted in the spectra of brain tissue following ischemia and reperfusion. A similar increase in low energy lipid region peaks is noted when comparing the spectra of adult brains to aged gerbil brains.

Testing for Age-Related Differences in Brains Detectable in the Near-IR. The first test for age-related differences utilized principal component regression (PCR) and six brains with a range in age of 15 months. The r^2 between age and the spectra was 0.97 (SEE = 2.19 months). The fitting residuals for the three older brains were larger than the younger three by an order of magnitude. The increase in residuals may arise from inherent differences in the aging process experienced by the animals.

In a subsequent test for age-related differences in the spectra of brain tissue, spectra of 10 adult control brains (see

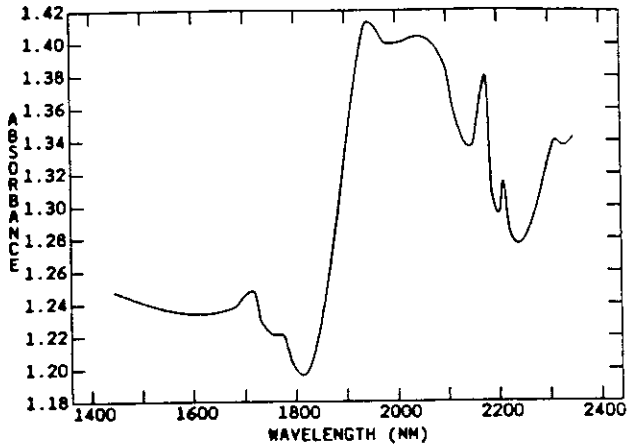

Figure 9. Average spectrum of 10 adult frozen control (no ischemia) brains.

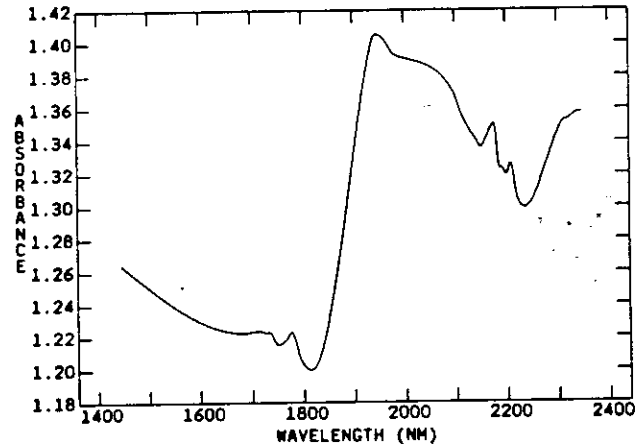

Figure 10. Average spectrum of 10 aged frozen control (no ischemia) brains.

Figure 9) were 14.1 SDs from a training set of spectra of aged control brains (see Figure 10 and Table I). Aging appears to increase the area of the peak in the lipid region near 1780 nm. When the adult brains were used as the training set, the aged brains were 23.7 SDs from the adults. The differences in the two distances reflects the fact that the aged brains are more variable in composition than the adult brains and, therefore, project as a larger group into wavelength hyperspace. One standard deviation is a larger Euclidean distance in a larger group, reducing the distance measured in standard deviations from this group. Nevertheless, even the smallest distance (14.1 SDs) represents a very small probability of confusing the adult brains with the aged ones.

Testing for Age-Related Oxidative Modification of Lipids and Proteins in Brain by Near-IR Spectrophotometry. The 20 brains used to create Figures 9 and 10 demonstrate a shift in lipid signals to longer wavelengths with aging that is consistent with either saturation of fatty acids and/or cis-to-trans isomerization of double bonds in fatty acids (compare the cis fatty acids to the trans and saturated fatty acids in Figure 2a–i). One mechanism consistent with the spectra that leads to saturation is a free radical chain reaction involving anti-Markovnikov addition to a carbon double bond. In this mechanism, peroxides serve as a source of chain-reaction initiators, while carbon double bonds in unsaturated fatty acids and in amino acids such as tryptophan, methionine, and cystine serve as chain propagators. Sulfur-containing amino acids could serve as sources of organosulfur radicals that participate in the chain initiation and propagation steps. Recombination of the organosulfur radicals could serve as the chain-halting step, leading to the

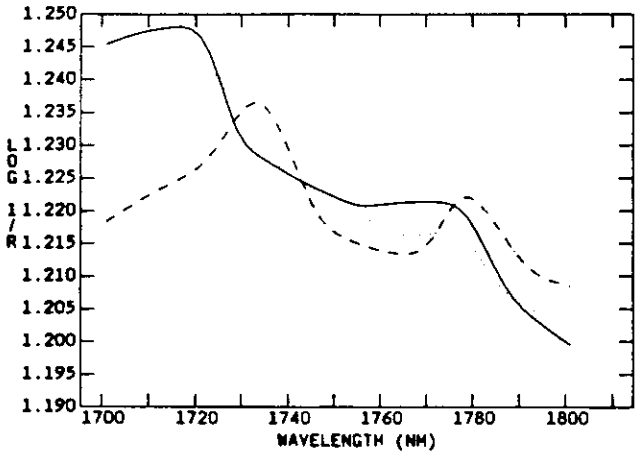

Figure 11. Average spectrum of 10 frozen adult control gerbil brains without ischemia (solid line), average spectrum of 10 frozen adult brains after 5-min ischemia and 1-h reperfusion (dashed line), and average spectrum of 10 frozen adult brains after 10-min ischemia and 1-h reperfusion (dot-dashed line).

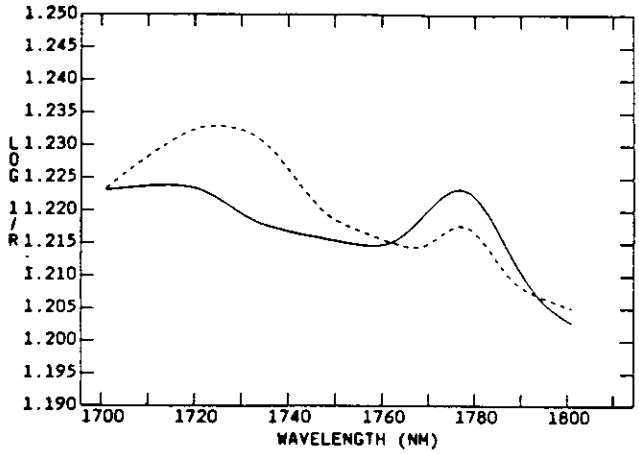

Figure 12. Average spectrum of 10 frozen aged control gerbil brains without ischemia (solid line) and average spectrum of 10 frozen aged brains after 5-min ischemia and 1-h reperfusion (dashed line).

formation of new amino acids such as cysteine and to the modification of peptide and lipid structures.

Metabolic enzymes including glutamine synthetase are known to be inactivated by metal-catalyzed oxidation reactions. The loss of specific activity of glutamine synthetase parallels protein oxidation during reperfusion of the ischemia-lesioned gerbil brain and serves as an early indicator of brain tissue damage.[7]

Testing for Saturation and/or cis–trans Isomerization of Fatty Acids (That Occurs Because of Ischemia and Peroxidation during Reperfusion) by near-IR Spectrophotometry. Near-IR spectra of adult gerbil brains following transient ischemia and reperfusion share spectral features in common with aged gerbils. In fact, the near-IR spectra of the 10 adult gerbils whose brains underwent 10-min ischemia and 60-min reperfusion and the 10 aged gerbils whose brains underwent 5-min ischemia and 60-min reperfusion were the only brains that were completely indistinguishable from one another by the near-IR system and supercomputer (see Table I). The distance in SDs between the control brains and ischemic brains was functionally related to the duration of ischemia: the change from 5-min ischemia to 10-min ischemia in the adult animals roughly doubled the distance of the brain spectra from the controls regardless of whether control or ischemic brains were used for calibration.

Figure 11 compares the average spectrum in the lipid region of 10 adult control gerbil brains without ischemia to the following: (1) the average spectrum of 10 adult brains after 5-min ischemia and 1-h reperfusion, and (2) the average spectrum of 10 adult brains after 10-min ischemia and 1-h reperfusion.

Using the roots of the first derivative of the spectra to locate peak centers, 5-min ischemia shifted the high energy lipid peak at 1717 nm to 1721 nm. After 10-min ischemia, the high energy lipid peak appeared at 1733 nm, a bathochromic shift of 16 nm. The low energy lipid peak centered at 1770 nm in the controls showed a 4-nm bathochromic shift with 5-min ischemia and a 9-nm bathochromic shift with 10-min ischemia. These changes in the spectra are consistent with a reduction in cis lipid carbon–hydrogen stretches and an increase in trans and/or saturated carbon–hydrogen stretches.

Figure 12 compares the average spectrum in the lipid region of 10 aged control gerbil brains without ischemia to the average spectrum of 10 aged brains after 5-min ischemia and 1-h reperfusion. The ischemic event generated an average bathochromic shift of 9 nm in the high energy lipid peak but no shift at all in the low energy lipid peak. Overall, the aged gerbil brain spectral peaks are shifted toward lower energies in the lipid region with respect to the adult brain spectra. The additional bathochromic shift in one of the peaks probably indicates a further reduction in cis lipid carbon–hydrogen stretches and an increase in trans and/or saturated carbon–hydrogen stretches.

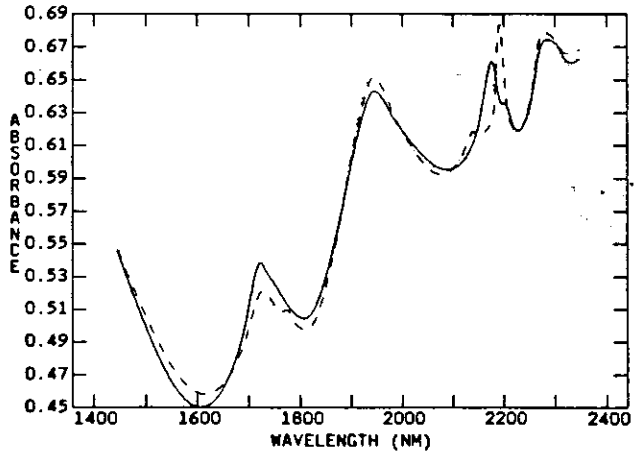

Figure 13. Brain spectra obtained noninvasively in vivo from a gerbil with shaved head before ischemia (control scan, solid line), after 10-min ischemia and 1-h reperfusion (dotted line), and after 4-h reperfusion (dot-dashed line).

To determine whether the changes observed in frozen excised brains could be observed in vivo, three aged gerbils were prepared surgically for ischemia, shaved, and scanned transcutaneously in vivo prior to 10-min ischemia and after ischemia at 1 h and 4 h of reperfusion. Figures 13 and 14 show that the maximum shift in peak area to longer wavelengths does not occur until at least 4 h of reperfusion.

Figure 15 shows the spectra from the third animal, which remain constant over the course of the experiment and show the low energy peak at 1780 nm. Edema (noted in the water band at 1940 nm) and persistent low energy lipid peaks (near 1780 nm) have been observed 24 h following a deliberately induced stroke. It is possible for a few animals to suffer strokes during the surgical procedure to implant a suture around the carotid artery as a result of vasospasm or some other alteration, and it appears that the third animal may have experienced such an ischemic event. It is important to note that prior to the development of noninvasive methods of assessing stroke-induced brain damage, an experimental animal that suffered a stroke before the experimental ischemia began would be blindly included with the other animals and might obscure

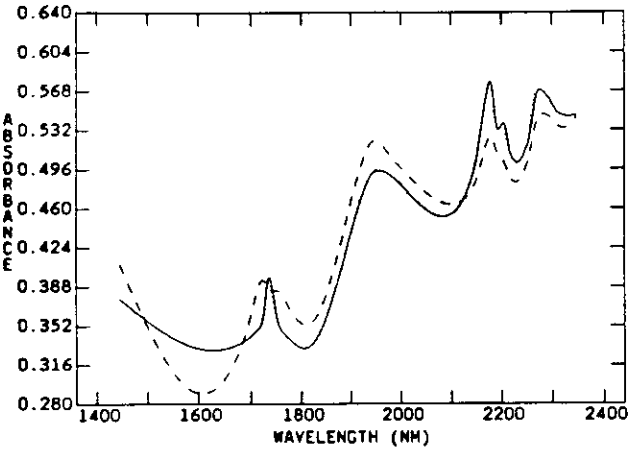

Figure 14. Brain spectra obtained noninvasively in vivo from a gerbil with shaved head before ischemia (control scan, solid line), after 10-min ischemia and 1-h reperfusion (dotted line), and after 4-h reperfusion (dot-dashed line).

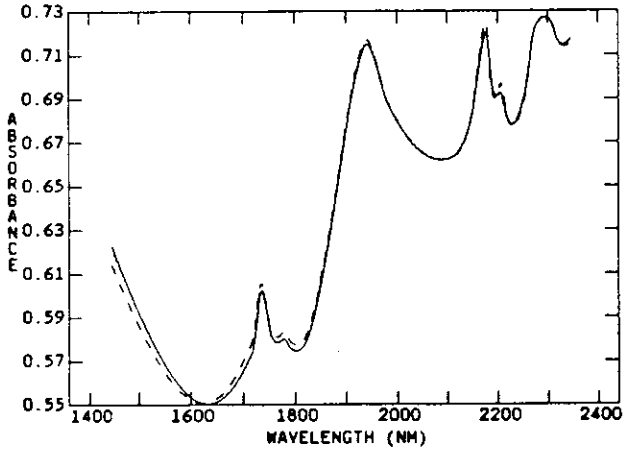

Figure 15. Brain spectra obtained noninvasively in vivo from a gerbil with shaved head. This animal suffered an apparent stroke during the initial surgery to position a suture around the carotid. A scan was obtained prior to experimental ischemia (solid line), after 10-min ischemia and 1-h reperfusion (dotted line), and after 4-h reperfusion (dot-dashed line). The experimental ischemia had no additional effect, and edema was already present along with low energy lipid peaks.

significant results.

Testing for Edema That Results from Ischemia/Reperfusion Injuries by Invasive and Noninvasive near-IR Spectrophotometry. The bound water peak near 2100 nm is more obvious in frozen brains than in living brains because the frozen brains are at dry ice temperature. Edema was noted in the spectra of 30 frozen brains that experienced ischemia. The amount of edema observed is functionally related to the duration of ischemia in brain spectra after multiplicative scatter correction. The 5-min ischemia in the adult brains in Figure 16 produces a larger water peak at 1940 nm than appears in the controls but a smaller water peak than the 10-min ischemia in the adult brains. Production of edema in aged brains is evident in Figure 17 which shows the average spectra of aged control brains and aged brains after 5-min ischemia. The mortality rate of 10-min ischemia in aged animals prevents the collection of 10-min ischemia/1-h reperfusion spectra.

In vivo scans obtained transcutaneously show that edema reached a maximum about 1 h following ischemia and then begins to regress (see Figures 13 and 14). A total of 76 adult and aged gerbils have been scanned in vivo, and Figures 13–15 represent well the range of changes that were observed in these spectra. The spectra from these 76 animals are now

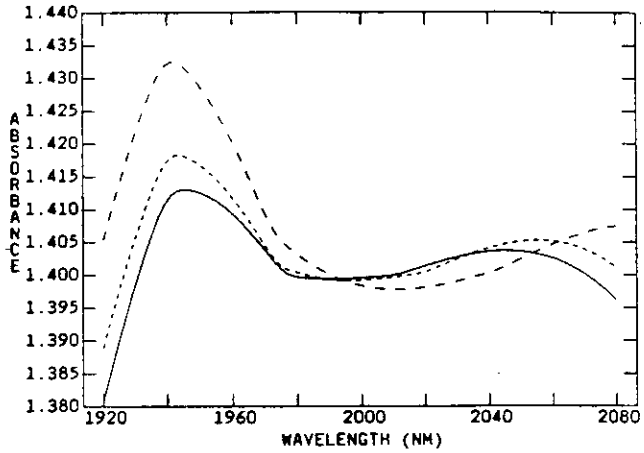

Figure 16. Average spectra of 10 adult frozen control brains (solid line), 10 adult frozen brains after 5-min ischemia and 1-h reperfusion (dashed line), and 10 adult frozen brains after 10-min ischemia and 1-h reperfusion (dot-dashed line).

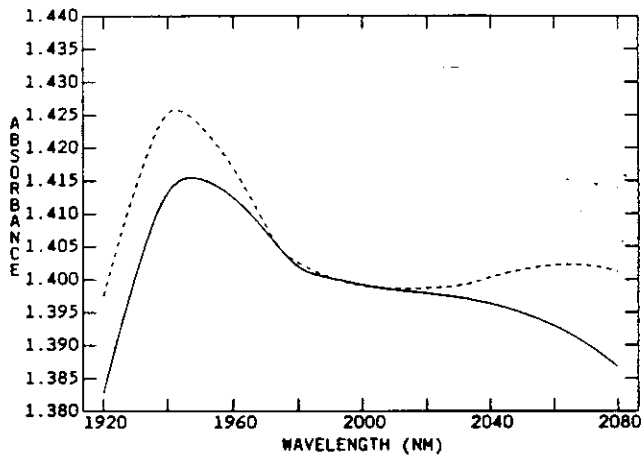

Figure 17. Average spectra of 10 aged frozen control brains (solid line) and 10 aged frozen brains after 5-min ischemia and 1-h reperfusion (dashed line).

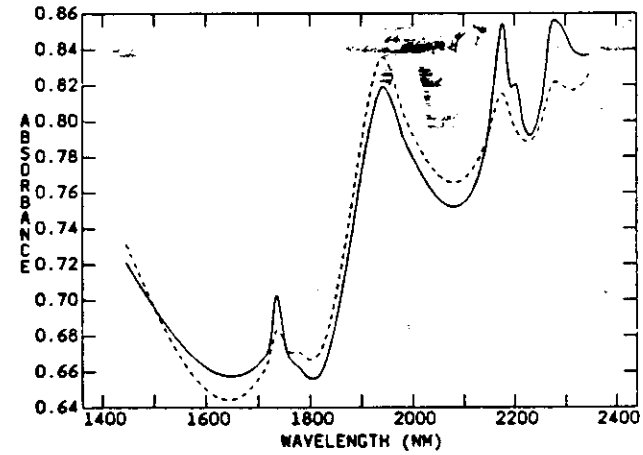

Figure 18. In vivo spectrum of a gerbil brain obtained transcutaneously (solid line) and with the skin removed from the skull (dashed line).

being used to develop a quantitative model for edema. At some point between 4-h reperfusion and 24-h reperfusion, edema begins to increase again. Future experiments will study the nonmonotonic behavior of edema in further detail.

The best near-IR determinations of brain age (in terms of standard errors) are obtained in young animals, which have thinner skulls. A broad spectrum of near-IR light from our spectrometer has been shown to penetrate through up to 4

mm of tissue,[12] however, making reliable measurements of brain spectra possible in gerbils of any age. Finally, two gerbils with an experimentally induced stroke were scanned in vivo with the skin and skull intact, and again with the skin removed exposing the skull. Figure 18 shows the typical scatter-corrected spectra obtained from one gerbil. Some of the peak structure in the protein region around 2200 nm is lost with the removal of the skin. The lower energy lipid peak near 1800 nm, observed following ischemia and reperfusion, is intensified by removal of the skin, as is the peak at 1940 nm due to edema. These are basically the same stroke-induced changes observed in the frozen and transcutaneous spectra.

CONCLUSION

The near-IR analytical method has numerous applications in aging and stroke research, including the determination of age from brain spectra, simultaneous multicomponent analysis of lipids and proteins, quantification of edema, and transcranial scanning of the brain in vivo. Near-IR spectrometry is well-suited for continuous measurements of brain status in research subjects and patients. Sample-handling hardware that makes sample presentation more reproducible has been constructed to realize these applications. Novel algorithms designed for parallel processors are also used to interpret spectral data and make spectra of individual samples more reproducible. Near-IR scanning of brains in vivo simplifies the testing of therapeutic drug candidates by reducing the number of animals required, by allowing each animal to be used as its own control, and by excluding outlier animals (such as those that have had a stroke before the experiment) from the experimental design. The application of near-IR video imaging technology should soon permit localization and analysis of the core and penumbra of stroke and the prediction of short-term memory deficit from the spectra of injured brains.

(12) Cassis, L. A.; Lodder, R. A. Near-IR imaging of atheromas in living arterial tissue. *Anal. Chem.*, in press.

ACKNOWLEDGMENT

This work was supported in part by the National Institutes of Health through Grants HL45143, AG10836, AG09690, and NS23307; the National Science Foundation through NYI Award 9257998 and STI-9108764; a grant from the Glenn Foundation for Medical Research, and the University of Kentucky Center for Computational Sciences (through a fellowship to Y.Z.).

RECEIVED for review August 21, 1992. Accepted February 8, 1993.